Fast reflectivity imaging in 3D using SAFT

N.V. Ruiter, M. Zapf, T. Hopp, and H. Gemmeke

Karlsruhe Institute of Technology, Karlsruhe, Germany
E-mail: nicole.ruiter@kit.edu

Abstract

The computational burden for 3D Synthetic Aperture Focusing Technique (SAFT) is large as for each voxel the delay for each acquired A-scan has to be calculated, e.g. $O(N^5)$ for N^3 voxels and N^2 A-scans. For 3D reconstruction of objects which are large in terms of the wavelength, e.g. $\geq (100\ \lambda)^3$, the computation of one volume takes several days on a current multicore PC. If the 3D distribution of speed of sound is applied to correct the delays for objects with varying speed of sound the computation time increases further. This overview paper presents the implementations for 3D SAFT developed by the KIT group and discusses their computational performance.

Keywords: 3D SAFT, reflectivity imaging, GPU, acceleration

1 Introduction

The KIT's 3D USCT system [1] has a semi-ellipsoidal aperture with 628 emitters and 1413 receivers, see Figure 1. The aperture's semi-axes are 0.13 m and 0.16 m. Four emitters and nine receivers are grouped into one transducer arrays system (TAS). 157 TAS are uniformly distributed on the surface of the aperture. The device, the aperture and patient positioning are shown in Fig. 1. Approx. spherical wavefronts are generated by using a single emitter at 2.5 MHz with approx. 50% bandwidth. Rotational and translational motion of the complete sensor system, so-called aperture positions, creates further virtual positions of the ultrasound transducers. The data acquisition is carried out with an FPGA-based system, which can store up to 80 GB of A-scans.

Reflection, attenuation and speed of sound images can be reconstructed from the same raw data set. For reconstruction of reflectivity volumes, i.e. qualitative imaging of the gradient of the acoustic impedance, a 3D synthetic aperture focusing technique (3D SAFT) is applied.

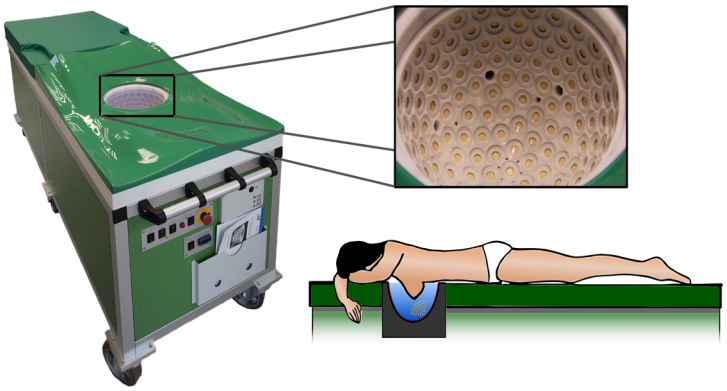

Figure 1: KIT 3D USCT with patient bed (left), transducer aperture (top right) and patient position (bottom right).

The computational burden for 3D SAFT is large as for each voxel the delay for each acquired A-scan has to be calculated, e.g. $O(N^5)$ for N^3 voxels and N^2 A-scans. For 3D reconstruction of objects which are large in terms of the wavelength, e.g. the female breast with diameters $\geq (100\ \lambda)^3$, the computation of one volume takes several days on a current multicore PC. For acceleration we developed a fast 3D SAFT implementation using multiple GPUs [2], reducing the computing time up to several minutes for a breast in resolution comparable to MRI.

Yet, for reflectivity volumes of high resolution up to $(0.5\ \lambda)^3$ speed of sound correction is necessary as the breast possesses a large range of speed of sound values [3], causing the images to defocus when a constant speed of sound is assumed. Incorporating speed of sound and attenuation correction in the GPU-based SAFT reconstruction increases the image quality significantly [4,5], but leads also to a significant reduction of computational performance. A time of flight interpolation based GPU implementation (TOFI-SAFT) [6] was developed which accelerates our previous GPU implementation of speed of sound corrected SAFT by a factor of 7 with only minor reduction of image quality. The approximation allows reconstructing speed of sound and attenuation corrected SAFT images as fast as non-corrected SAFT. In this paper the applied methods for accelerating SAFT and some results of phantoms and clinical cases are shown.

2 Methods

2.1 3D synthetic aperture technique

The applied reconstruction algorithm for reflectivity images is the 3D synthetic aperture focusing technique (SAFT), which can be described by the following equation:

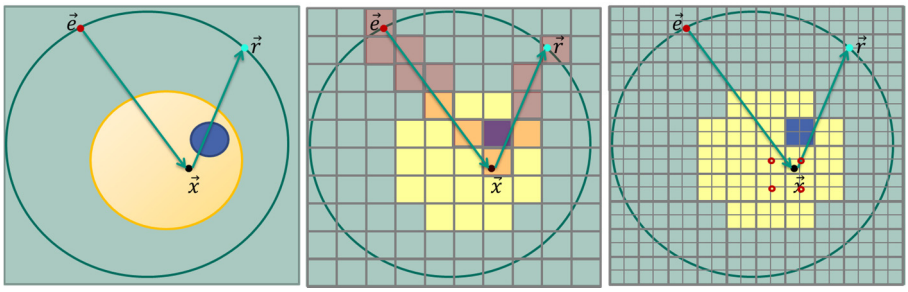

Figure 2: Simplified 2D diagrams of SAFT reconstruction: On the left the geometry with emitter $\vec{e}$, point $\vec{x}$ and receiver $\vec{x}$ and a circular breast (beige) with inclusion (blue). In the center the same geometry overlaid with low resolution speed of sound map and approximated paths for calculation of the average speed of sound. On the right overlaid with higher resolution grid for reflectivity imaging and red marks indicating the voxels of the speed of sound map used for interpolation of the average speed of sound $\hat{c}_{path(\vec{e},\vec{x},\vec{r})}$ for point $\vec{x}$.

$$I(\vec{x}) = \sum_{\forall(e,r)} \left(\frac{1}{att} T(A_{(e,r)} tof) \right) \text{ with } tof = \frac{\|\vec{e}-\vec{x}\|+\|\vec{x}-\vec{r}\|}{\hat{c}}, \quad (1)$$

where I denotes the reconstructed qualitative volume of local impedance-differences, $\vec{x}$ the reconstructed point, att is the attenuation of the ultrasound signal from emitter to point $\vec{x}$ to receiver, T contains the pre-processing steps, $A_{e,\mathrm{r}}$ is the A-scan acquired at emitting position $\vec{e}$ and receiving position $\vec{r}$. The time tof is the time of flight from emitter $\vec{e}$ to the point $\vec{x}$ and to receiver $\vec{r}$. The equation is valid for small attenuation, weak point scatterers, and spherical emittance. SAFT calculates at each image point the mean of all reflections which might originate from this position. Norton and Linzer [7] showed that for ideal conditions, i.e. continuous aperture, isotropic point scatterers and no attenuation, SAFT solves the inverse problem of calculating the local impedance differences. A simplified setup is shown in Figure 2 left.

For the simplest reconstruction, the harmonic mean of the speed of sound $\hat{c}$ may be assumed to be constant, e.g. the speed of sound of water at the temperature measured during image acquisition. Often the attenuation att is ignored, i.e. set to 1.

Acquiring unfocused ultrasound facilitates new possibilities for signal preprocessing, as the data can be accessed before the focus of emission is generated. For reconstruction of clinical cases we either use a matched filter only, or apply the preprocessing "Adapted Matched Filter" [8] described in the following, especially if images of lower resolution are reconstructed. First, a matched filter is applied to increase the signal-to-noise ratio, by correlating the signal with the known pulse shape. This is followed by an envelope transformation and detection of the local maxima. To cope with the phase aberrations the resulting signal is convoluted by a pulse with an adapted lower bandwidth.

In summary, the preprocessing is

$$T\big(A(t)\big) = locMax\big(\big|H\big(A(t) * p(t)\big)\big|\big) \otimes p_{opt,\tau_{new}}(t), \tag{2}$$

where $locMax$ denotes the local maximum, H the Hilbert transform, $*$ the cross-correlation operator, $p(t)$ the known pulse form, and $\otimes$ the convolution operator.

The optimal pulse $p_{opt,\tau_{new}}(t)$ for reflectivity imaging was introduced by Norton and Linzer [7] with

$$p_{opt,\tau_{new}}(t) = \frac{2\sqrt{\pi}}{{\tau_{new}}^3}\left[1 - 2\left(\frac{\pi \cdot t}{\tau_{new}}\right)^2\right] \cdot e^{-\left(\frac{\pi \cdot t}{\tau_{new}}\right)^2}, \tag{3}$$

where τ_{new} is the new pulse duration, i.e. the main lobe of the optimum pulse. For example if the main lobe of the optimal pulse is set to $2\,\mu s$, this corresponds to a Full Width Half Maximum (FWHM) of the point spread function of approx. 1.5 mm, and is comparable to the resolution of an breast MR image.

2.2 Speed of sound and attenuation correction

Assuming constant speed of sound can lead in large objects with varying speed of sound to wrong scaling, spatial displacement and even defocusing of the image contents. For USCT approaches where the "paths" of the sounds, i.e. direction of the sound wave travelling through the object, vary greatly due to the wide spatial distribution of the transducers defocusing is prominent. For example Figure 6 left shows a cylindrical gelatin phantom (Ø 10 cm) with one embedded bonding wire (Ø 0.5 mm). The gelatin has a speed of sound of approx. 1550 m/s, the surrounding water 1490 m/s. Center left and right show slices of 3D SAFT reconstructions without and with sound speed correction. The improvement of the image quality is significant. For the KIT 3D USCT the real speed of sound may maximally deviate from the constant assumption by 0.28 m/s for high resolution reconstructions [9]. On the contrary not accounting for refraction effects does not significantly reduce the image quality when the speed of sound is corrected [10].

For 3D SAFT with speed of sound and attenuation correction the intensity $I(\vec{x})$ of a voxel at $\vec{x}$ is calculated by

$$I(\vec{x}) = \sum_{\forall(e,r)} \left(\frac{1}{att_{path(\vec{e},\vec{x},\vec{r})}} T(A_{(e,r)} tof)\right) \text{ with } tof = \frac{\|\vec{e}-\vec{x}\|+\|\vec{x}-\vec{r}\|}{\hat{c}_{path(\vec{e},\vec{x},\vec{r})}}, \tag{4}$$

where $att_{path(\vec{e},\vec{x},\vec{r})}$ is the attenuation and $\hat{c}_{path(\vec{e},\vec{x},\vec{r})}$ is the mean sound speed on the direct path from $\vec{e}$ to $\vec{x}$ and $\vec{r}$, i.e. the average values are calculated from all voxels which lie on the straight lines connecting $\vec{e}$ and $\vec{x}$ and $\vec{r}$ and $\vec{x}$, respectively.

2.3 Acceleration using GPUs

Equation (1) shows that SAFT can be parallelized easily, i.e. each A-scan and / or each voxel can be calculated independently. The elementary operations of the reconstruction, i.e. addition, multiplication and even square root operations, can be implemented efficiently. However the large number of operations which are necessary for USCT applications causes SAFT to be computing intensive, as for each voxel of a breast sized volume in submillimeter resolution the delay tof of each A-scan has to be calculated. E.g. for a hemispherical breast of 10 cm radius, a voxel size of (0.5 mm)³ and 5 million A-scans more than 10^{14} tof calculations are necessary.

Our GPU implementation of 3D SAFT without correction assumes $\hat{c}$ to be constant and $att = 1$. Acceleration is achieved by calculating the volumes with parallel GPUs. The maximum performance on eight GTX 590 is 107 GVA/s, where 1 GVA/s denotes 10^9 voxel and A-scans processed per second, and the calculation of the above example takes 37 min.

For high resolution SAFT images a speed of sound correction is necessary to focus the image content. Additionally, attenuation correction increases the contrast of the SAFT images. For corrected SAFT reconstruction $att_{path(\vec{e},\vec{x},\vec{r})}$ as the attenuation and $\hat{c}_{path(\vec{e},\vec{x},\vec{r})}$ as the mean sound speed on the path from $\vec{e}$ to $\vec{x}$ and $\vec{r}$ are calculated using reconstructed attenuation and speed of sound images from the same acquired data. For performant calculation of the corrected SAFT volumes on GPUs the paths are approximated by Bresenham's algorithm [11] and calculated on voxel grids of low resolution. In Figure 2 the center and right diagrams show an example. Path calculations using up to factor 20 lower resolution than the SAFT resolution still result in acceptable focusing [4]. With correction for speed of sound and attenuation variations, the performance on eight GTX 590 GPUs decreases to 34 GVA/s when using 128³ voxels for the speed of sound and attenuation volumes [9] and the calculation takes 2 h.

2.4 Time of flight interpolated synthetic aperture focusing technique

For clinical studies or even clinical practice a 2 hour calculation poses a long delay between data acquisition and image availability. Hence a fast alternative is necessary, allowing the important speed of sound correction. Reducing the number of calculated tof would result in a lower resolution of the volumes, which is not desirable. The alternative is to reduce the amount of operations per tof calculation. TOFI-SAFT reduces the number of operations by calculating the exact tof only for a small subset of voxels, i. e. the tof calculation in equation (1) is only carried out for the voxels corresponding to the reduced speed of sound resolution. The tof of all other high resolution voxels is calculated by linear interpolation using the neighboring base points of exact tof values. Figure 3 shows an example for a simple 2D case.

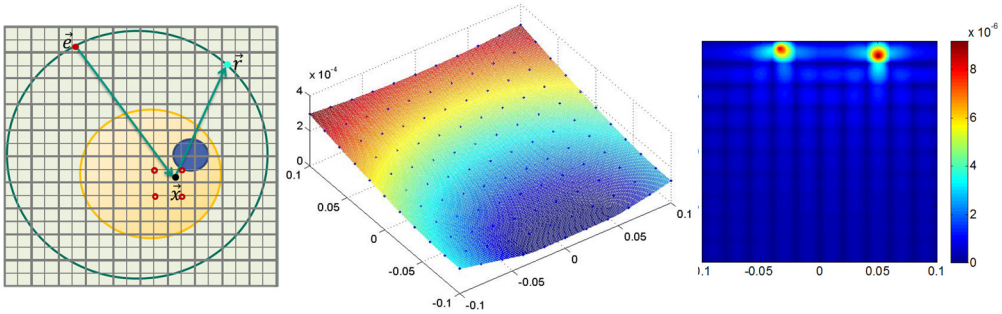

Figure 3: Principle of TOFI-SAFT simplified in 2D. Left: Emitter $\vec{e}$ and receiver $\vec{r}$ on a ring aperture with radius of 10 cm using the same setup as in Fig. 2. The tof of pixel $\vec{x}$ is interpolated for this emitter receiver combination. Overlay of grid of pixels with a low resolution speed of sound image (bold grey lines) and a high resolution SAFT image (thin grey lines). Red dots mark the spatial positions of neighboring base points with tof calculation from equation (4) applied for linear interpolation of tof for pixel $\vec{x}$. Center: $tof_{\vec{e},\vec{r}}(\vec{x})$ for the given example, the resolution of speed of sound is (2 cm)² and of SAFT is (1 mm)². Dark blue dots indicate the position of the base points. Right: Error map of calculated and linearly interpolated tof with mean of 0.6 µs, median of 0.4 µs and standard deviation of 0.7 µs. The areas of large errors up to 9 µs are located near the transducers and outside of the breast. Speed of sound is assumed to be constant at 1500 m/s.

A more general analysis in 3D of the errors made by this approximation showed that large errors are mainly located outside the breast as the error drops quickly with increasing distance to the transducers and does not significantly decrease the image quality [6].

For implementation of TOFI-SAFT within our GPU framework, the base points for exact tof calculations are chosen to coincide with the voxels of the speed of sound volume, which is applied for correction in lower resolution, i.e. factor 5 to 10. The tof of the high resolution voxels for the reflectivity volumes, which do not coincide with the base points, are linearly interpolated using the tof of neighboring base points. For GPU implementation the linear interpolation can be carried out very effectively in texture memory units.

TOFI-SAFT achieves a maximum performance of 104 GVA/s on the GPU server with eight GTX 590, which is a speed up of factor 3 compared to the corrected SAFT. It approaches the maximum performance of 107 GVA/s of the uncorrected SAFT reconstruction. Tested on one newer generation GPU, GTX Titan, TOFI-SAFT can be even faster than uncorrected SAFT: a GPU server of eight GTX Titans would result in a maximum performance of 210 GVA/s for uncorrected SAFT, 62 GVA/s for corrected SAFT and 442 GVA/s for TOFI-SAFT which is a speed up of more than factor 7. This increase in performance is due to 3.5 times more texture units in GTX Titan compared to GTX 590. Thus for the above example with a semispherical breast of 10 cm radius, a voxel size of (0.05 mm)³, 5 million A-scans and 80^3 base points TOFI-SAFT could be calculated in 16 min on eight GTX Titan GPUs.

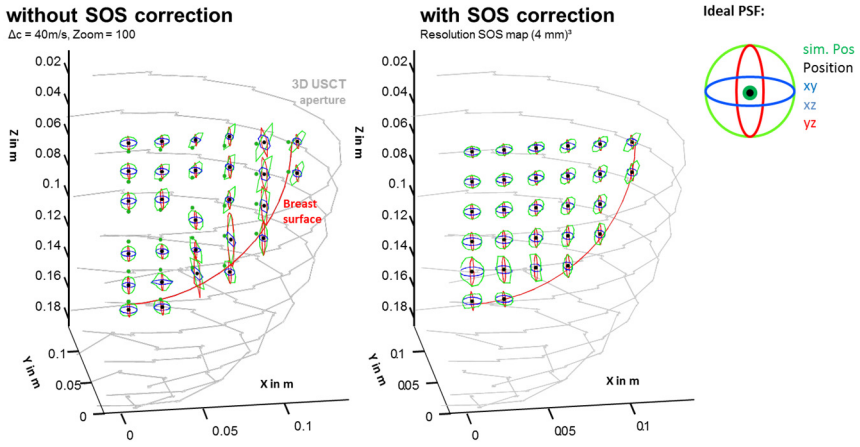

Figure 4: Resulting point spread functions of 28 simulated point scatterers within a hemispherical breast of 20 cm diameter and speed of sound of 1540 m/s in 1500 m/s water. The PSFs are scaled wit a factor of 100 for better visibility.

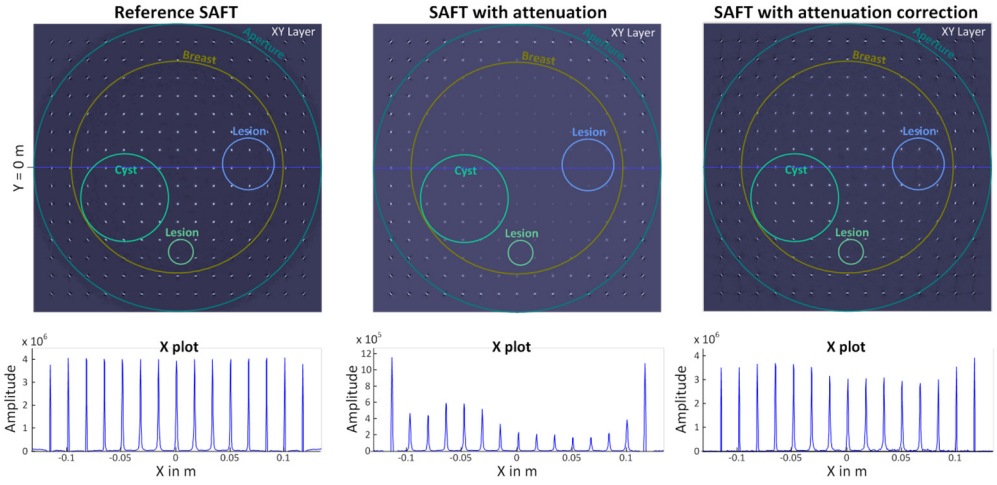

Figure 5: Comparison of reconstructions of 255 simulated point scatterers for (left) not attenuation, (center) attenuation simulated but not taken into account for the reconstruction, and (right) simulated and reconstructed attenuation. The top rows shows slice images of the reconstruction and the bottom row contour plots of the scatterers at y = 0m (blue line). The breast had 20 cm diameter and 0.5 dB/cm attenuation, the cyst 0.0009 dB/cm and 8 cm diameter, and the lesions 0.1 dB/cm and 2 and 4 cm diameter. No noise was added to the simulations.

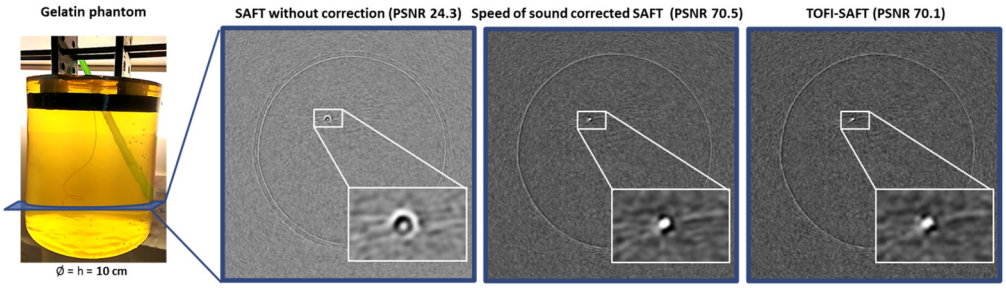

Figure 6: Comparison of SAFT reconstructions of the gelatin phantom with nylon thread. Left: Photo of Phantom. Center left: SAFT reconstruction without correction. Center right: Slice image with speed of sound corrected SAFT (PSNR 70.5). Right: Slice of TOFI-SAFT (PSNR 70.1).

3 Results

For evaluation of the speed of sound correction a simulation of a worst case scenario was used. Figure 4 shows a diagram of the resulting point spread functions (PSF) of 28 simulated point scatterers within a breast with 20 cm diameter and speed of sound of 1540 m/s in 1500 m/s water. The PSFs are scaled by a factor of 100 for better visibility. Without speed of sound correction the mean displacement of the points is 6 mm, the mean width of the PSF is 0.5 mm and the relative contrast, i.e. percentage of Peak-Signal-to-Noise-Ratio (PSNR, $PSNR = \frac{\max(I)}{\sigma(I)}$) to PSNR of the ground truth, i.e. reconstruction of simulation without speed of sound difference, is 16%. The speed of sound correction approach using a SOS map with (4 mm)³ resolution results in a mean displacement of the reconstructed points of 0.06 mm, a mean PSF of 0.28 mm, and a relative contrast of 85%. Figure 6 center left and center right show experimental results.

Similarly, for evaluation of the attenuation correction 255 point scatterers within a 20 cm breast were simulated. Resulting slice images and contour plots are shown in Figure 5. The breast tissue was simulated at 0.5 dB/cm attenuation, the cyst at 0.0009 dB/cm and had 8 cm diameter.The lesions had a diameter of 2 and 4 cm with an attenuation of 0.1 dB/cm. No noise was added to the simulations. The percentage of the relative standard deviation (STD) of the reflectivity of the scatterers was measured as quality metric and normalized to the maximum amplitude of the reconstructed point scatterers in the reference, i.e. no attenuation simulated. The measure resulted in 34 % of relative STD for the non-corrected SAFT and 9% for the corrected SAFT. For evaluation of TOFI-SAFT A-scans for 54 evenly distributed point scatters within one quarter of the maximum sized breast (hemisphere with 10 cm radius) were simulated for the 3D USCT aperture with speed of sound of the background of 1500 m/s and 1460 m/s for the breast tissue.

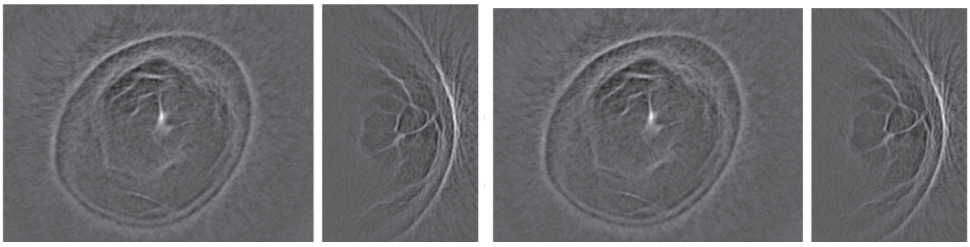

Figure 7: 3D USCT slice images of reflectivity volumes reconstructed with corrected SAFT (left) and with TOFI-SAFT (right) for patient data. The imaged breast has a maximum diameter of approx. 18 cm. The reduction of image contrast in terms of peak signal to noise ratio (PSNR from left to right: 32.1, 43.9, 32.1, 43.8) is very small.

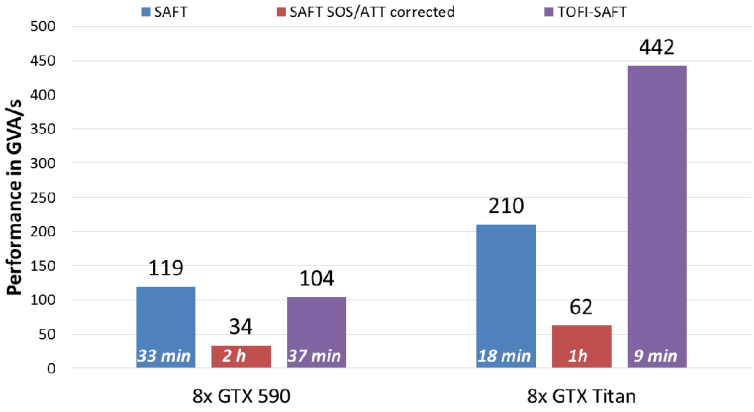

Figure 8: Performance of the three 3D SAFT approaches for two different generations of GPUs in GVA/s. The durations in minutes and hours respectively were calculated for an example of 444^2 x 266 voxels for reflectivity volumes with 128^3 base points, and 10^7 A-scans. The GTX Titan has a large number of texture units for interpolation, in this case the performance of TOFI-SAFT including speed of sound correction can even surpass the performance of SAFT without speed of sound correction.

The A-scans were then used to reconstruct speed of sound corrected SAFT volumes without and with TOFI approximation. The voxel size of the SAFT volumes was $(0.05\ \text{mm})^3$ and 128^3 base points were applied. The mean full width half maximum was 0.34 mm for TOFI-SAFT compared to 0.33 mm with full speed of sound corrected SAFT and the relative contrast was 0.98. Thus the errors introduced by the approximation are not significant for the resulting image quality.

For experimental evaluation a phantom consisting of a gelatin block of cylindrical shape (height and diameter 10 cm) containing a nylon thread of diameter of 0.2 mm, see Figure 6, was imaged. The phantom was reconstructed with a voxel size of $(0.4\ \text{mm})^3$ and 128^3 base points. The image contrast in terms of PSNR of the approximation was only reduced by 0.6%

compared to the full calculation of all tof. Comparing speed of sound corrected SAFT and TOFI-SAFT for clinical data resulted also in only small degradation of the image quality, see Figure 7.

Figure 8 summarizes the performance values for the different SAFT approaches. For calculation of the duration of SAFT the example setup was to reconstruct a SAFT volume of 444^2 x 266 voxels, with 128^3 base points, i.e. resolution of the attenuation and SOS maps, and 10^7 A-scans (N~900).

4 Discussion and conclusion

In this paper an overview of three approaches for fast calculation of 3D SAFT for 3D USCT at KIT was presented and the motivation to apply speed of sound and attenuation correction was given. For clinical applicability, i.e. calculation of breast volumes in a couple of minutes, a new approximation based approach for speed of sound corrected 3D SAFT enables a significant acceleration of reconstructions for reflectivity volumes with only minor reduction of image quality. The type of applied GPU limits the performance by increased memory requirements and texture units for interpolation, thus high end GPUs are required, especially when using TOFI-SAFT.

Using quad-core CPUs and a cluster of eight GPUs allowed us for the first time to calculate volumes in less than 10 min, enabling the application of the method in clinical studies. While readout of the full raw data is important during the development state, for clinical practice a stand-alone system outputting reconstructed images only would be sufficient. For application in clinical practice, however, we also considered reuse of the device's built-in FPGA-based data acquisition system (DAQ) through reconfiguration. Due to the dated FPGAs the speed up was only marginal. Yet 3D SAFT using new generation FPGAs was shown to be nearly as performant as using GPUs [12]. For future development of the 3D USCT technology scalability and a good performance-per-power ratio become very important. Therefore we will consider FPGAs for future applications. Today, with the available FPGA technology real-time imaging is not possible at reasonable efforts and costs. However, we expect that even real-time image reconstruction will be possible by the year 2020, roughly following Moore’s law.

References

[1] Ruiter, N.V., Zapf, M., et al.: “First Results of a Clinical Study with 3D Ultrasound Computer Tomography.” Proc. IEEE Internat. Ultrasonics Symp., (2013).

[2] Kretzek, E., Zapf, M., Birk, M., Gemmeke, H., Ruiter, N.V., “GPU based acceleration of 3D USCT image reconstruction with efficient integration into MATLAB,” Proc. SPIE 8675, Medical Imaging 2013: Ultrasonic Imaging, Tomography, and Therapy, page 86750O (2013).

[3] Ruiter, N.V., Schnell, R., Zapf, M., Gemmeke, H., “Phase aberration correction for 3D Ultrasound Computer Tomography images,” 2007 IEEE Ultrasonics Symposium, pps. 1808–11 (2007).

[4] Kretzek, E., Ruiter, N.V., “GPU based 3D SAFT reconstruction including phase aberration,” Proc. SPIE 9040, Medical Imaging 2014: Ultrasonic Imaging and Tomography, pages 90400W (2014).

[5] Kretzek, E., Hopp, T., Ruiter, N.V., “GPU-based 3D SAFT reconstruction including attenuation correction,” Proc. SPIE 9419, Medical Imaging 2015: Ultrasonic Imaging and Tomography, pages 94190E (2015).

[6] Ruiter, N.V., Kretzek, E, Zapf, M., Hopp, T., Gemmeke, H., “Time of flight interpolated synthetic aperture focusing technique,” Proc. SPIE 10139, Medical Imaging 2017: Ultrasonic Imaging and Tomography, 101390Q (2017).

[7] Norton, S., Linzer, M., “Ultrasonic reflectivity imaging in three dimensions: Reconstruction with a spherical array,” Ultrasonic Imaging, vol. 1 (3), pp. 21031, 1979.

[8] Ruiter, N.V., Schwarzenberg, G.F., Zapf, M., Gemmeke, H., “Improvement of 3D ultrasound computer tomography images by signal pre-processing,” Proc. IEEE UFFC Symp., pp. 852-855, 2008.

[9] Kretzek, E., “Optimierung von Bildgebungsverfahren für die 3D-Ultraschall-Computertomographie,” Ph.D Thesis, KIT, 2015.

[10] Hopp, T., Zapf, M., Gemmeke, H., Ruiter, N.V., “Experimental evaluation of straight ray and bent ray phase aberration correction for USCT SAFT imaging,”, Proc. SPIE Medical Imaging 2018, in press.

[11] Bresenham, J.E., “Algorithm for computer control of a digital plotter,” IBM Systems Journal, 4(1), pps. 25-30, (1965).

[12] Birk, M., Kretzek, E., Figuli, P., Weber, M., Becker, J., Ruiter, N.V., "High-Speed Medical Imaging in 3D Ultrasound Computer Tomography," in IEEE Transactions on Parallel and Distributed Systems, 27(2), pp. 455-67, 2016.